Renewable and Sustainable Energy Reviews 38 (2014) 821–833

Contents lists available at ScienceDirect

Renewable and Sustainable Energy Reviews

journal homepage: www.elsevier.com/locate/rser

Screening analysis of metal hydride based thermal energy storage systems for concentrating solar power plants

Claudio Corgnale *, Bruce Hardy, Theodore Motyka, Ragaiy Zidan, Joseph Teprovich, Brent Peters

Savannah River National Laboratory, Aiken, SC 29808, USA

ARTICLE INFO

Article history:
Received 3 February 2014
Received in revised form
8 May 2014
Accepted 6 July 2014
Available online 24 July 2014

Keywords:
Concentrating solar power
Thermal energy storage
Hydrogen storage
Metal hydrides
Techno-economic analysis

ABSTRACT

Concentrating solar power plants represent a competitive option to produce electric power only if equipped with suitable thermal energy storage. Metal hydride material-based thermochemical hydrogen storage is a very attractive solution to store high temperature solar thermal energy. A literature review of some of the past and more recent investigations on using metal hydrides for thermal energy storage has been carried out. Based on findings from this review and new material property data, a preliminary material techno-economic analysis was performed to select the most promising candidate metal hydrides as well as to examine their behavior under different operating conditions. The performance was evaluated adopting simplified system models and the results were compared against the US Department of Energy targets including installed cost, exergetic efficiency, operating temperature and volumetric energy density. Selected sensitivity analyses for the most promising materials have also been carried out in order to evaluate the influence of solar plant and material properties on the overall system installed cost. Results demonstrated that the selected storage systems, based on currently available metal hydride high temperature materials (i.e. $NaMgH_3$, TiH_2 and CaH_2), are able to achieve and exceed many of the targets such as volumetric energy density (25 kWhth/m^3) and operating temperature (600 °C). Material modifications as well as heat exchange system improvements are also discussed in the paper, with the aim of reducing the overall thermal energy storage specific cost and helping to meet and exceed all of the targets.

Contents

Abbreviations: CSP, Concentrating Solar Power; DOE, USA Department of Energy; HTMH, High temperature metal hydride; LTMH, Low temperature metal hydride; MH, Metal Hydride; PCF, Plant Capacity Factor; PP, Power plant; SRNL, Savannah River National Laboratory; TES, Thermal Energy Storage

* Corresponding author. Tel: +1 8036179689.
E-mail addresses: claudio.corgnale@gmail.com, claudio.corgnale@greenway-energy.com (C. Corgnale).

http://dx.doi.org/10.1016/j.rser.2014.07.049
1364-0321/

1. Introduction

Power plants driven by renewable sources represent one of the main options to produce electric power without local greenhouse gas emissions. Among the different possibilities for large scale plants, CSP systems are positioned to become a major source of renewable-generated electricity in the United States [1]. This is especially due to the fact that they have a higher potential for providing dispatchable power among all the different renewable options [2–5]. However only CSP plants equipped with TES systems have the potential to reach the DOE SunShot Initiative solar electricity production target of 0.06 $/kWh [6] similar to conventional power plants [3,7]. The three types of TES systems, being developed today, store energy either as: (1) sensible heat, (2) latent heat from material phase change or (3) thermochemical heat, using the heat released (or absorbed) during chemical reactions occurring inside the material [2,3].

Among the third type of TES systems, MH based systems are a very attractive choice, showing strong potential to achieve the DOE SunShot Initiative TES targets [6], which include exergetic efficiency, operating temperature, cost and volumetric energy density. More information on the specific DOE SunShot TES targets and their current values can be found in Section 3 of this paper. Compared to other TES systems MH technology has several attractive features, including full reversibility, high gravimetric and volumetric energy density. Although some MH/TES systems can be costly recent material discoveries allow for the potential for much lower system cost [8]. An example of a medium temperature TES systems, based on MgH_2 material, has a reported gravimetric energy density approximately 18 times higher than that of molten salts [8].

To effectively design and build a TES system based on MH materials, different processes need to be examined, involving momentum, mass and energy transport phenomena, coupled with kinetics and thermodynamics of the materials involved. In addition, experimental activities are needed in order to collect the material property data (such as kinetics, thermodynamics, hysteresis, and stability with cycling etc.) and to develop new materials or modify existing materials for the specific conditions. Experiments need to be carried out to verify the performance of the material under different operating conditions and for extended operating periods (e.g. cycling capacity).

The objective of this paper is to review the previous work on MH-based TES systems and to analyze that work in light of new recently discovered MH materials and today's CSP TES systems cost and performance targets. The analysis performed in this study uses a screening analysis to examine different possible TES systems based on MH materials. The aim of the analysis is to: (1) select candidate MH's, which have the potential to meet the targets; and (2) evaluate the performance of the selected materials under different operating conditions. The screening model can also be applied to identify the properties of an 'ideal material' system, capable of achieving all of the targets. In addition, the results are useful to guide experimental effort toward needed material modifications. The use of screening tools does not take the place of more detailed numerical simulations and experimental studies needed to fully evaluate and describe the TES system. However, starting with less costly and time consuming effort can be helpful and needed as part of the scientific methodology to pave the way to more detailed numerical and experimental studies. Therefore, before carrying out detailed numerical and experimental campaigns, it is necessary and more practical that a screening analysis of the possible MH materials can focus both the experimental and numerical efforts by selecting a reasonable number of high potential candidate materials.

2. Metal hydride-based TES systems

This section describes the use of MH's to store solar thermal energy in a CSP plant. The section also illustrates the cycle of the heat storing and recovery when solar radiation is available and when it is not.

Solar power plants that have the potential of meeting the DOE targets have been identified by the DOE as baseline renewable source based power systems [9,6]. One of the most common plants is based on the steam Rankine cycle. The solar plant, shown in Fig. 1, is comprised of the solar capturing and concentrating section, the TES section (based on the MH system concept), and the power plant (based on a steam Rankine cycle). The same MH based thermal energy storage system can be adapted for use with other power plants (e.g. Brayton cycle), with only a few minor variations.

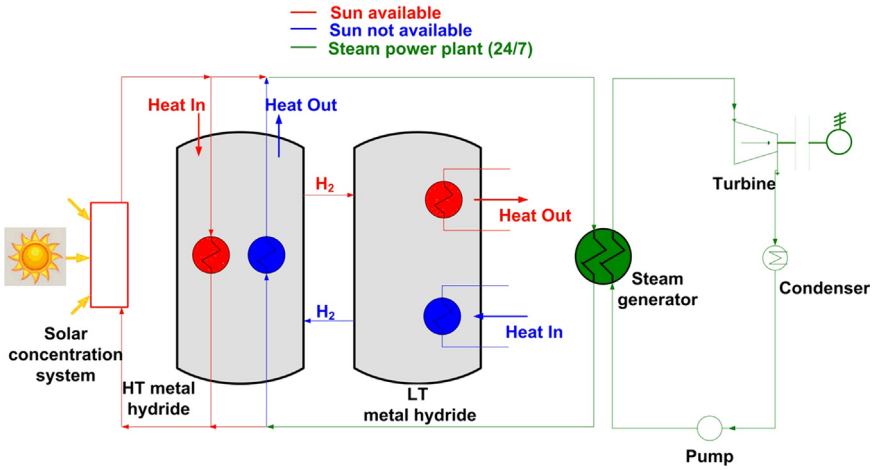

Fig. 1. Schematic of a Rankine cycle based-CSP plant with a TES system comprised of both HT Metal Hydride and LT Metal Hydride materials.

Nomenclature

A	Heat transfer area (m^2)
C_{AHE}	Installation costs ($)
C_{AM}	Additional material costs to modify and allocate the metal hydride material ($)
C_{HE}	Heat transfer system installed cost ($)
C_{HEF}	Free On Board (FOB) cost of the heat transfer system ($)
C_{HEPVS}	Heat transfer and pressure vessel system specific installed cost ($/kWhth)
C_M	Metal hydride material installed cost ($)
C_{MS}	Metal hydride material specific installed cost ($/kWhth)
$\overline{C_{P1c-2c}}$	Average specific heat of the heat transfer fluid between station 1c and 2c (Fig. 3) (kJ/kg-K)
$\overline{C_{P1d-2d}}$	Average specific heat of the heat transfer fluid between station 1d and 2d (Fig. 3) (kJ/kg-K)
C_{PV}	Pressure vessel (wall) cost ($)
C_{RM}	Cost of the raw metal hydride material ($)
Cs	TES system specific cost ($/kWhth)
D_1	Heat transfer fluid tube diameter (Fig. 2) (m)
D_2	Single metal hydride cylindrical structure diameter (Fig. 2) (m)
Ech	Chemical exergy content (kWhth)
E_{th}	Thermal energy stored (kWhth)
Eth	Thermal exergy content (kWhth)
h	Specific enthalpy (kJ/kg)
L	Length of the heat exchanger (m)
$\overline{m}$	Heat transfer fluid mass flow rate (kg/s)
M	Metal hydride mass (kg)
M_{H2}	Mass of hydrogen to be stored in the metal hydrides (kg)
n_T	Number of tubes of the heat exchanger
s	Entropy (kJ/kg-K)
T	Temperature (K or °C)
T_0	Reference temperature for exergy calculations (298 K)
U	Heat transfer coefficient (W/m^2-K)
V	Metal hydride material volume (m^3)
W_{el}	Average electric power produced by power plant during the year (MW)
wf	High temperature metal hydride weight capacity (kg_{H2}/kg_{MH})
W_{th}	Thermal power exchanged between the Metal Hydride and the heat transfer fluid (MW)

Greek letters

Δt_s	Storage time (h)
ΔT	Mean temperature difference between the heat transfer fluid and the metal hydride (°C)
ΔH	Metal hydride enthalpy, heat of reaction (kJ/mol_{H2})
ΔS	Metal hydride entropy of reaction (kJ/mol_{H2}-K)
ΔG	Gibbs energy (kJ/mol_{H2})
η_{PP}	Power plant efficiency
ρ	Metal hydride material bulk density (kg/m^3)
ψ	Exergetic efficiency

Subscripts

$1c$	Property referred to station 1 during charging (1c in Fig. 3)
$1d$	Property referred to station 1 during discharging (1d in Fig. 3)
$2c$	Property referred to station 2 during charging (2c in Fig. 3)
$2d$	Property referred to station 2 during discharging (2d in Fig. 3)
c	Referred to the charging process
$cond$	Heat transfer coefficient referred to conductive heat transfer process
$conv$	Heat transfer coefficient referred to convective heat transfer process
d	Referred to the discharging process
$HTMH$	High temperature metal hydride
$LTMH$	Low temperature metal hydride

The power plant is expected to work 24/7, with the power level determined by its PCF, mainly depending on the storage time and the plant location. The TES system stores and releases the needed thermal energy to maintain continuous operation of the power section. The thermal energy storage system shown in Fig. 1 is comprised of two MH materials with two different enthalpies operating at different temperatures and its conceptual behavior is described below.

During the day ('Sun available' in Fig. 1), the available surplus solar power is stored in the TES. The HTMH has a high enthalpy value and works at high temperature, allowing it to store large amount of heat by using solar heat to release hydrogen (endothermic process) and store it in the LTMH. As LTMH absorbs hydrogen (exothermic process) it releases low temperature heat, which is extracted from the TES system. During the night or times when additional thermal energy is required to run the power plant ('Sun not available' in Fig. 1), the process is reversed. Hydrogen is allowed to flow from the LTMH and be absorbed by the HTMH exothermally providing the needed heat at high temperature to the steam generator. The higher energy density that can be provided by the use of metal hydride systems has been shown to have a mass energy density on the order of 15–20 times higher than molten salts-based TES systems [8]. This can substantially lower the size and the capital cost of many CSP TES systems. Using only small pressure changes, hydrogen can be transferred from one metal hydride system to another to exchange large quantities of heat at high temperature with the external heat transfer fluid. Hydrogen moves between the two beds by the pressure gradients generated after heating or cooling the system through suitable thermal management of the TES units and choosing suitable material pairs. This simple exchange results in a self-sustaining system, without the use of additional hydrogen compression system that would increase the electric power consumption.

One of the main applications of MH materials is to store reversibly hydrogen to be used as fuel to produce mechanical power (e.g. in internal combustion engines) or electric power (e.g. in fuel cells) after reacting with oxygen (or air). However several other applications exist where the MH heat of reaction can be used directly, without exploiting the hydrogen chemical content (heating value) through its oxidation with oxygen. Heat is available from the exothermic reaction of hydrogen with a MH and the temperature can be varied with the operating pressure of the system. The applications where the MH heat of absorption can suitably be utilized range from refrigeration applications, to solar thermal energy storage [10–12]. The use of MH materials for high temperature solar thermal energy storage is of great interest due

to their unique material properties. Lithium (Li) based MH was one of the first hydrides examined for this purpose. Caldwell et al. [13] proposed at the end of 1960s the integration of LiH-based solar TES system with solar parabolic concentrator systems. The proposed system was designed to provide continuous heat to a satellite power conversion system deployed in near-earth orbit. Experimental tests (with a MH bed of about 0.45 kg of LiH) were conducted for 190 hours highlighting a good performance of the TES system. A maximum temperature of 760 °C was achieved during the tests. The authors concluded that the LiH based TES system would be very attractive for space applications or to balance the solar source availability when only solar energy is available. Hanold and Johnston [14] proposed the use of Li material based heat storage systems for power plants and, more particularly, as a heat storage arrangement for a Stirling cycle engine. A conical concentrator was designed and connected to the MH based TES, integrated with the Stirling engine, reaching temperatures around 700 °C. Different materials were tested. Lithium compounds such as lithium hydride, lithium hydroxide and lithium fluoride (with particular attention to lithium hydride) seemed to be the best materials, due to their high temperatures (>700 °C) and their high energy density, with a heat of fusion around 3500 kJ/kg [14].

More recently the attention has shifted to Mg-based solar TES systems, due to the lower cost of the Mg materials compared to Li hydride. After carrying out an overview of the methods for solar heat storage, Bogdanovic et al. [15] conclude that among the reversible metal-hydride–metal systems, the MgH_2 system is particularly attractive. This is due to its high hydrogen content and the high energy content of the Mg–H bond. Experimental results of heat storage were obtained by coupling a storage system based on MgH_2 with a low-temperature metal hydride storage system (i.e. $MmNi_5$[2] material) [15], highlighting a good performance of the system. Two other aspects, namely the catalytic hydrogenation and the doping of magnesium powders, were emphasized by Bogdanovic et al. [15] as important aspects of the system. Several studies were carried out to compare the performance of Ni-doped MgH_2 system against the performance of un-doped MgH_2 material for high temperature solar energy storage. After an analysis of different possible doping techniques, Bogdanovic et al. [16] conclude that the mechanical mixing of Mg powder with Ni powder in the dry state 'turned out to be by far the simplest and least expensive doping method'. Bogdanovic et al. [17] showed that Ni-doped Mg–MgH_2 materials had excellent cyclic stability and high hydrogenation rates suitable for applications such as solar generation of heat and cold, heat pumps and hydrogen storage. They showed [17] that the material can be used as an economic option for the purpose of reversible thermochemical high temperature heat storage in the temperature range of 450–500 °C. The material reached heat storage capacities of 0.6–0.7 kWh/kg-Mg (2160–2520 kJ/kg-Mg) [17].

Felderhoff and Bogdanovic [18] described two possible applications of the MgH_2 based TES system for high temperature CSP plants. The first system describes the direct integration of the MgH_2 bed with a steam generator for use in a Rankine cycle. The volume of the experimental device is about 19 L with 14.5 kg of Ni doped Mg. The max operating temperature is 450 °C with a max pressure of 50 bar and a max thermal power of 4 kW exchanged to produce steam [19]. The MgH_2 bed is paired both with low temperature hydrogen pressure tank and with a LTMH material based on Ti–Fe–Cr–Mn [19].

The second application described in Ref. [18] investigates the adoption of Mg based TES systems in Stirling engine-based thermochemical power plants. This is an evolution of the previous concept, with the HTMH system providing the needed heat when sunlight is unavailable. A preliminary small solar power station system was built at the Max Plank Institute during the 1990s [18,20]. The main components are a solar radiation concentrator, a cavity radiation receiver, a heat pipe system for heat transfer, a Stirling engine, a MgH_2 TES coupled with a hydrogen pressure tank or an LTMH tank based on Ti–Fe–Cr–V–Mn material [20]. To transfer the heat two potassium heat pipes were used [20]. The first laboratory systems contained about 20 kg of Mg powder with a storage capacity of about 12 kWhth and reaching operating temperatures in the range 300–480 °C [20].

Other possible Mg-based materials have recently been investigated as possible elements of HTMH solar TES systems. These materials include: Mg–Fe hydride, Mg-Ni hydride, Mg–Co based hydride [21] and Na–Mg hydride [22]. The Mg–Ni/Mg_2NiH_4 material demonstrated a good cyclic stability with weight capacity of about 3% and reaching energy densities of 916 kJ/kg at temperatures of 230–330 °C [21]. The Mg–Fe/Mg_2FeH_6 material showed good cyclic stability at temperatures of 480–550 °C, corresponding to a pressure range of about 60–100 bar and achieving weight capacity values on the order of 5.4% [21]. Mg–Co–H material has a theoretical weight capacity on the order of 4–4.5%, depending on the hydrides formed in the Mg–Co–H system [21]. However two plateau regions were found by Reiser et al. [21]: the first plateau has a hydrogen content up to 2.5%, while the second plateau provides an additional 2.5% to about 3.7% hydrogen capacity. The material operating temperatures are on the order of 450–550 °C with pressure on the same order of MgFe based hydride [21]. A comparison among Mg–Fe, Mg–Ni and Mg–Co materials resulted in identifying the Mg–Fe compound as the most promising material for high temperature TES applications, due to its operating conditions, low material cost and high material weight capacity [21,23]. A more detailed investigation of the potential of Mg–Fe material as a high temperature TES material was given by Bogdanovic et al. [23]. The performance of the material is shown in Ref. [23] reported an excellent cycling stability at around 500 °C. The authors [23] also compared the performance of different Mg–Fe materials that were prepared starting from different initial Fe/MgH_2 ratios. Recently increasing attention has been paid to the adoption of $NaMgH_3$ material as a possible low cost high temperature TES system. Sheppard et al. [22] performed experimental tests to assess the performance of the perovskite-type hydride, $NaMgH_3$ under high temperature CSP plant conditions. The authors suggest the use of $NaMgH_3$ hydride at temperatures around 580–600 °C with a one step reaction, corresponding to pressures (on the order of tens of bar) lower than the other Mg-based materials [22].

Recently, some renewed interest has also been paid to Ca-based hydride to store high temperature solar thermal energy. Due to its very high heat of formation (at 950 °C the heat released during hydrogen absorption is 4494 kJ/kg [8]), there was early interest in using calcium hydride for thermochemical energy storage. Some authors [8] referred to one proposal to construct a CSP power plant at the end of 1970s with a 700 kWe output using a sodium loop to transfer the heat from the solar concentrator to the reactor. A CSP plant using calcium hydride as the storage material with a continuous output of 100 kWe system coupled to a Stirling engine has recently been investigated in Australia [24].

Possible candidate LTMH materials, to be paired with the corresponding HTMH material, are usually selected among the AB_5 and AB type materials. The AB_5 materials, based on MishMetal or Rare Earth materials (e.g. $MmNi_5$ or $LaNi_5$ materials), are materials that offer very good stability and cycling performance at low temperature (around 25 °C) with weight capacities on the order of 1–1.5%. The adoption of these materials as LTMH TES materials has been demonstrated in several solar applications [18,25]. Another possible AB_5 hydride is based on $CaNi_5$ material. Yonezu et al. [25] proposed dual LTMH beds with $CaNi_5$ coupled to

[2] Mish Metal – Ni_5 material

$MmNi_5$ through a heat pipe based heat exchanger. More recently Chumphongphan et al. [26] demonstrated better stability of Al doped $CaNi_5$ compared to the undoped material at 85 °C and 20 bar. The intermetallic AB type materials (usually TiFe based LTMH materials), are usually less expensive than AB_5 materials. Libowitz [27,28] reported on one of the first applications of AB materials for solar TES systems. This report shows the use of TiFe material for low temperature solar systems, analyzing the behavior under different operating conditions and for different configurations. The AB class of materials has excellent cycling properties with operating temperatures on the order of ambient temperature and weight capacities around 1–2% [27]. The $TiFeH_2$ hydride has recently been proposed as one of the best candidates LTMH at low pressures to be paired with the CaH_2 HTMH material by Buckley et al. [8]. A new class of low cost complex hydrides, sodium alanates ($NaAlH_4$), has been the focus of extensive research as hydrogen storage materials since Bogdanovic and Swickardi [29] demonstrated the reversibility of the reaction by catalyzing the reaction. This material has not been used as LTMH TES material yet. However sodium alanate has several properties that make the compound very attractive for this application. These properties will be discussed in the next sections of the document.

3. The MH-based TES system screening model

The DOE released specific technical targets for the CSP TES systems [6], reported here:

- TES operating temperatures higher than 600 °C to assure high efficiencies of the power plant,
- TES exergetic efficiency higher than 95%,
- TES specific cost lower than 15 $/kWhth, and
- TES volumetric energy density higher than 25 kWhth/m^3.

Based on the previous research work and the DOE requirements, a guiding screening analysis is needed in order to build a TES system that meets the targets.

A screening tool has been developed to screen and compare the most promising MH materials-based TES systems, having the potential to meet the DOE targets listed above. The selected MH systems have been examined and screened comparing their behavior against all the targets, including the specific cost, the exergetic efficiency, the operating temperature and the volumetric energy density. The tool can also be utilized to define the properties of the ideal MH material-based TES that can meet all the targets. This is useful for: (1) comparing the performance of the currently existing materials with that of the ideal materials; and (2) guiding future experimental research, in the event that none of the currently available MH materials can meet all of the DOE targets. The analysis has been carried out based on a techno-economic model of the TES system, described in the next sections.

3.1. The techno-economic model

One of the main objectives of the techno-economic analysis for the TES system is the evaluation of the system installed cost, compared to the economic target. The specific installed cost of the TES system (Cs) has been assessed accounting for: (1) the cost of the MH materials (C_M), (2) the cost of the heat transfer system (C_{HE}), (3) the cost of the pressure vessel walls (C_{PV}). Thus:

$$Cs = (C_M + C_{HE} + C_{PV})/E_{th} \quad (1)$$

The methodology to evaluate the thermal energy stored (E_{th}) is reported in the Annex at Eq. (a1).

The installed cost of the MH material (C_M) is given by

$$C_M = C_{RM} + C_{AM} \quad (2)$$

The first term (C_{RM}) is the cost based on the raw cost of the material. This cost is given by the specific cost ($/kg) of the raw material of the metal hydride multiplied by the mass of metal hydride needed to store the hydrogen. The methodology to evaluate the HTMH and LTMH masses and volumes is reported in the Annex at Eqs. (a3)–(a6). The second term (C_{AM}) accounts for all the additional manufacturing, work and handling needed to locate the MH inside the tank. Based on previous experience with small scale stationary applications, C_{AM} has been assumed equal to 20% of the raw cost of the material (C_{RM}) [30].

The shell and tube heat exchanger concept has been assumed as the baseline heat transfer system to evaluate the cost of the heat transfer system (C_{HE}). This baseline system is assumed because it is a well-known and common baseline technology and it also allows for future possible variations and improvements. The heat transfer fluid, which exchanges the thermal power with the MH, flows inside the tubes with the MH material packed around the tubes.

A simplified steady state 1-D radial model is presented here, that has been adopted to evaluate the heat transfer area. The model is based on cylindrical coordinate geometry. The MH bed has been modeled as a series of structures comprising cylindrical tubes, with the fluid flowing inside them (Fig. 2 shows the single cylindrical structure). The heat exchange process for each cylindrical structure has been modeled comprising: (1) the conductive thermal resistance ($1/U_{cond}$), due to the heat transfer process inside the MH material; and (2) the convective thermal resistance ($1/U_{conv}$), due to the heat transfer process occurring inside the tubes, as illustrated in Fig. 2. The conductive thermal resistance can be expressed as follows, as function of MH material thermal conductivity (k), heat transfer fluid tube diameter (D_1) and the single MH material structure diameter (D_2) (see Fig. 2). Fixed temperatures at the heat transfer fluid tube diameter (D_1) and at the MH material structure diameter (D_2) have been assumed as boundary conditions of the problem

$$\frac{1}{U_{cond}} = \frac{D_1 \ln(D_2/D_1)}{2k} \quad (3)$$

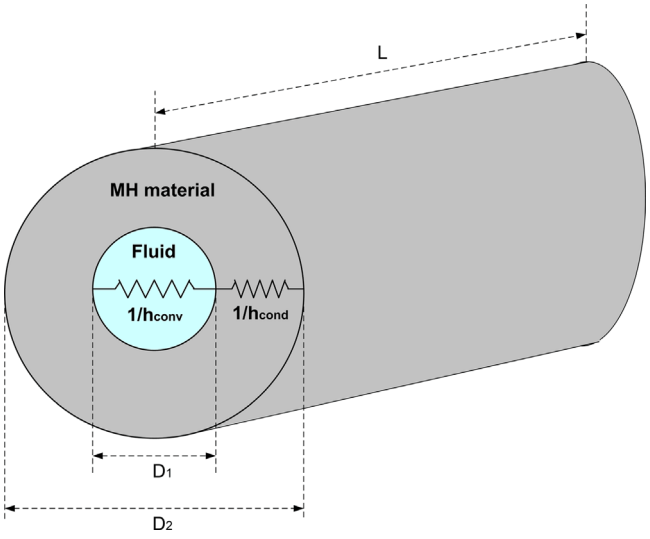

Fig. 2. Schematic of the tube and metal hydride (MH) material structure for a cylindrical geometry thermal model, with the MH material packed around the tube carrying the heat transfer fluid. The structure is repeated n-times inside the storage tank.

As a preliminary assumption a constant value has been considered for the convective thermal resistance (U_{conv}) based on typical coefficient values for such applications[3].

The overall heat flux Wth, can be expressed as a function of convective heat transfer coefficient (Ucond), convective heat transfer coefficient (Uconv) number of tubes (nT), heat transfer fluid tube diameter (D_1), length of the heat exchanger (L) and mean temperature difference between the fluid and the MH (ΔT):

$$Wth = \left(\frac{1}{(1/U_{cond})+(1/U_{conv})}\right) n_T \pi D_1 L(\Delta T) \quad (4)$$

The volume occupied by the metal hydride, determined by the CSP plant properties and the material properties and easily evaluated by Eqs. (a4) and (a6) in the Annex, gives an additional constraint.

The data and the assumed degrees of freedom of the problem are: D_1, k, U_{conv}, ΔT and L, with their values provided in the following sections. The unknown quantities are D_2 and n_T. The unknown values can be evaluated from Eqs. (3) and (4) with the constraint given by the volume occupied by the MH material (Eqs. (a4) and (a6) in the Annex).

The heat transfer area (A) is equal to:

$$A = n_T \pi D_1 L \quad (5)$$

Once the heat transfer area has been assessed, the installed cost of the shell and tube heat exchanger can be estimated based on traditional factored method approaches [31]. Thus the component cost (C_{HE}) is given by

$$C_{HE} = C_{FHE} + C_{AHE} \quad (6)$$

The component FOB cost (C_{FHE}) has been evaluated from the cost of a reference heat exchanger. The reference heat exchanger cost depends on its area, the value A, and its conditions (1 bar operating pressure, CS material and straight tube geometry heat exchanger). To evaluate the FOB cost, the initial reference cost has been modified adopting suitable cost factors. These cost factors account for the actual heat exchanger working conditions (i.e. operating pressure), materials and heat exchanger geometry. Stainless Steel (SS) has been considered as the current baseline material for the specific MH system. However, other materials, capable of withstanding higher temperature can be considered when needed. Straight tubes heat exchanger geometry is considered for all the MH systems. The reference cost and the additional cost factors have been assessed using data based on References [32,33] and suitably modified to match the actual system condition and configuration.

The term C_{AHE} includes all the installation costs of the component such as piping, instrumentation, concrete and insulation, as well as labor etc. The installation costs have been assessed as percentage of the FOB component cost (C_{FHE}) using proper factors. By this approach, the component cost (C_{HE}) can be expressed as shown in Eq. (7)

$$C_{HE} = f C_{FHE} \quad (7)$$

The installation factor (f) accounts for all the additional costs needed to install the component

For the specific application, an installation factor (f) equal to approximately 1.5 has been used. This value is based on the available databases [32] and on the size of the heat exchangers as well as on previous experience gained from small scale stationary MH bed applications [30].

The outer shell of the hydride bed (e.g. pressure vessel) cost has been assessed, adopting the same factored method approach. The approach is similar to that adopted to evaluate the cost of the heat exchangers. The pressure vessel FOB cost (C_{PV}) has been evaluated as a function of working conditions (pressure), vessel material (SS is the baseline material) and the size of the vessel (diameter and length) using the databases available in Reference [32]. An additional 25% of void volume has been included when estimating the vessel dimensions to allow the expansion/contraction of the MH material during charging and discharging process, following best practices [30].

System cost is one of the main factors to be considered for any future implementation of MH as a TES system. Performance, material and system properties and material cost are the main aspects affecting the system cost. The CSP performance determines the amount of thermal energy to be stored and consequently the amount of hydrogen to be stored. The MH material thermochemical and economic properties (namely the reaction enthalpy, weight capacity, working conditions, material price etc.) determine the MH mass and the material cost as well as the cost of the pressure vessel and heat exchanger. The heat transfer system properties, in terms of heat transfer coefficients, determine the heat transfer area and in turn the cost of the heat exchanger.

3.2. Exergetic efficiency model

Another TES system target is related to its exergetic efficiency performance. Fig. 3 shows the MH storage system interfaced with the high temperature heat transfer fluid heat exchanger. Fig. 3a shows the heat storage process when excess thermal power is available with hydrogen moving from the HTMH to the LTMH. The exergetic input is the thermal exergy related to the high temperature heat transfer fluid. The chemical exergy related to the endothermic hydrogen discharging reaction from the HTMH represents the exergy available in the TES system. Fig. 3b shows the heat release process with hydrogen moving from the LTMH to the HTMH. In this case the exergetic input is the chemical exergy, from the hydrogen charging reaction in the HTMH. The heat transfer fluid thermal exergy represents the exergy available from the TES system.

During heat storage, Eth_c represents the total exergetic input available from the high temperature heat transfer fluid and Ech_c represents the total chemical exergy stored in the metal hydride bed. For a stationary process the exergetic efficiency (ψ_c) is given by:

$$\psi_c = \frac{Ech_c}{Eth_c} \quad (8)$$

with ψ_c being the exergetic efficiency of the heat storage process. The two exergy terms (Ech_c and Eth_c) can be written in terms of Gibbs energy variation between initial and final state, as reported below[4]. The thermal exergy (Eth_c) is:

$$Eth_c = \dot{m}_c \Delta t_s (h_{2c} - h_{1c} - T_0(s_{2c} - s_{1c})) \quad (9)$$

The term $\dot{m}_c$ represents the heat transfer fluid mass flow rate and Δt_s is the storage time. The Gibbs function is expressed in terms of enthalpy variation between point 2c (h_{2c}) and point 1c (h_{1c}) and entropy variation between point 2c (s_{2c}) and point 1c (s_{1c})

The heat transfer fluid mass flow rate ($\dot{m}_c$) can be evaluated, by the energy balance equation applied to the heat transfer process, as the ratio between the thermal power exchanged between the metal hydride and the heat transfer fluid (W_{th}) and the specific enthalpy variation between points 2c and 1c ($\overline{C_{p1c-2c}}$ represents the average specific heat between point 1c and point 2c):

$$\dot{m}_c = \frac{W_{th}}{\overline{C_{p1c-2c}}(T_{1c} - T_{2c})} \quad (10)$$

[3] Traditional straight tube convective heat transfer correlations (such as Dittus and Boelter correlation) could also be adopted to evaluate U_{conv}.

[4] The kinetics energy term as well as potential term, referred to the reference exergetic state, have been assumed negligible.

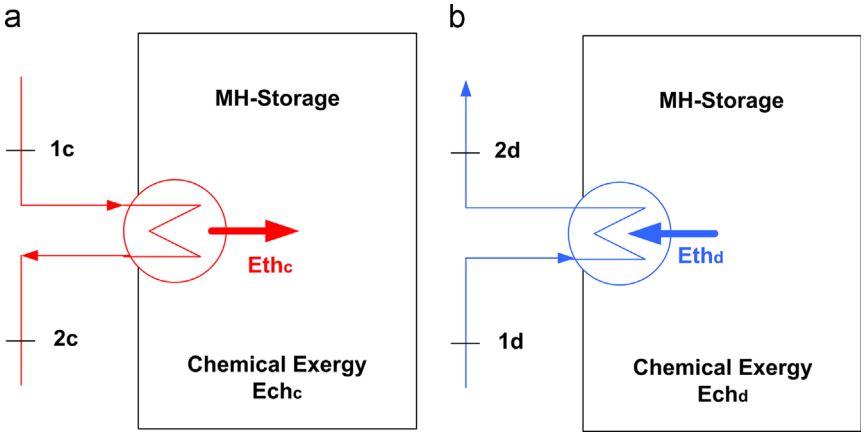

Fig. 3. Schematic of the MH-based TES system interfaced with the HT heat transfer fluid: during the heat storage (a) the heat transfer fluid provides the thermal power (Eth_c is its thermal exergy) to the HTMH which reacts (Ech_c is the reaction chemical exergy) to discharge hydrogen; during the heat release (b) the heat transfer fluid collects the thermal power (Eth_d is the thermal exergy) from the metal hydride which reacts (Ech_d is the reaction chemical exergy) to charge hydrogen.

The conditions at point 1c and point 2c have been evaluated assuming the values of the mean temperature difference between the heat transfer fluid and the metal hydride (ΔT) and the maximum temperature of the heat transfer fluid in the plant (T_{1c}), which varies according to the specific TES system.

The following approach has been adopted to evaluate the chemical exergy available from the thermochemical reaction in the hydride. In general the chemical exergy of a chemical compound (Ec), referred to the standard exergetic conditions, can be evaluated as follows:

$$E_c = \Delta G_f + \sum_i n_i E_{cs_i} \tag{11}$$

ΔG_f (kJ/mol) is the compound Gibbs energy of formation. n_i is the stoichiometric coefficient for the element i in the compound. E_{csi} (kJ/mol) is the standard chemical exergy of the element i. The second term allows the chemical exergy of the compound to be evaluated referring to the exergetic standard conditions. In general the values in the tables available from [34,35] can be used to evaluate the reference state of the single elements. However, for the MH specific case, the thermodynamic properties relate to the overall reaction, referring to enthalpy and entropy variation between final and initial stage. This allows the Eq. (11) to be simplified and the chemical exergy term (Ech_c) can be evaluated as reported in Eq. (12)

$$Ech_c = M_{H2}(\Delta H_c - T_0 \Delta S_c) \tag{12}$$

M_{H2} indicates the mass of stored hydrogen and ΔH and ΔS represent the reaction enthalpy and entropy during the heat storage process.

The exergetic efficiency for heat released from the TES system (ψ_d) can be written as

$$\psi_d = \frac{Eth_d}{Ech_d} \tag{13}$$

Ech_d represents the total exergetic input available from the chemical reaction (hydrogen absorption), Eth_d represents the thermal exergy in the heat transfer fluid. Following the approach previously described for the heat charging phase, the two terms reported in Eq. (13) can be written and evaluated as follows (Eqs. (14)–(15)):

$$Eth_d = \dot{m}_d \Delta t_s (h_{2d} - h_{1d} - T_0(s_{2d} - s_{1d})) \tag{14}$$

The term $\dot{m}_d$represents the heat transfer fluid mass flow rate and Δt_s is the storage time. The Gibbs function is expressed in terms of enthalpy variation between point 2d (h_{2d}) and point 1d (h_{1d}) and entropy variation between point 2d (s_{2d}) and point 1d (s_{1d})

$$\dot{m}_d = \frac{W_{th}}{\overline{C_{p1d-2d}}(T_{2d} - T_{1d})} \tag{15}$$

$$Ech_d = m_{H2}(\Delta H_d - T_0 \Delta S_d) \tag{16}$$

M_{H2} indicates the mass of stored hydrogen and ΔH and ΔS represent the reaction enthalpy and entropy during the heat release process.

The following assumptions have been made for the present analysis:

1. The assumed heat transfer fluid is air. Air is suitable for a wide range of operating temperatures that can reach values up to 900–1000 °C. Previous studies in the literature report the use of air or inert gases (e.g. helium) as intermediate fluid to exchange the heat between the solar tower and the interfaced equipment of the plant [36,37].
2. No hysteresis has been assumed for the various metal hydride materials. This is due to the fact that many materials still lack accurate thermodynamic data on their hysteresis during charging and discharging of hydrogen. With this assumption: $\Delta H_c = \Delta H_d$ and $\Delta S_c = \Delta S_d$. A decrease of exergetic efficiency of approximately 1% is likely expected once the hysteresis effect is included, but this depends on the MH material considered.

The final total exergetic efficiency (ψ) of the system, examining the charging (ψ_c) and discharging (ψ_d) process, becomes

$$\psi = \psi_c \psi_d = \frac{Ech_c}{Eth_c}\frac{Eth_d}{Ech_d} \tag{17}$$

With assumption 2, the overall efficiency, reported in Eq. (17), becomes equal to Eth_d/Eth_c. However, the two contributions of Eq. (17) need to be considered to evaluate the separate influence of charging and discharging processes and to assure that ψ_c and ψ_d are less than 1. The problem is completely defined, without any degree of freedom once the fluid conditions at points 1c (and 1d) and 2c (and 2d) have been defined and the thermodynamic properties of the MH's are known.

3.3. Methodology and assumptions

Based on data available in the literature [8,38,39] and on the previous considerations about the available MH materials for solar applications, potential MH candidate materials for both HTMH and LTMH systems have been identified. They are reported in Table 1,

including the properties needed for the screening analysis. These materials represent the majority of the currently available MH materials for high temperature ($>500\,^{\circ}C$) solar applications. These materials have the potential to meet or closely approach the techno-economic targets. The intrinsic property values, which are independent of the application, are extracted from the references reported in the Table 1. If the intrinsic property values are missing, they are obtained and assessed from profiles and tables available from Reference [40].

The best HTMH material candidates are those with: (1) high reaction enthalpy; (2) high working temperatures, which affect the efficiency of the power plant; (3) high hydrogen capacity, which determines the mass of the HTMH (i.e. the HTMH material cost); (4) low raw material cost, in order to reduce the HTMH system cost. Other available HTMH materials, such as KAl-based and ZrMn-based hydrides, have not been included as potential candidates due to their high raw material cost. The best LTMH materials are those with: (1) low reaction enthalpy, which determines the LTMH thermal power to be exchanged with the heat transfer fluid; (2) low working temperature, which allows the heat to be exchanged with a low temperature source; (3) high weight capacity, which determines the mass of the LTMH (i.e. the LTMH material cost); (4) low raw material cost, in order to reduce the LTMH system cost. Other LTMH materials, such as LaNi-based, V-based and CaNi-based materials, are available for solar applications but have not been included as candidate materials due to their high material price or instability with cycling. The bulk density of the materials has been assessed based on their crystal density and assuming a void fraction on the order of 0.5, which is a typical value for MH tanks. The weight capacity values reported in Table 1 refer to the theoretical material capacity. However, practical values have been adopted in the techno-economic analysis based on the data reported in the literature and based on previous experience with selected materials (e.g. a practical capacity of 7% has been considered for MgH_2 material, based on Ref. [41]).

The screening analysis of the MH-based TES systems has been performed in steps. A screening of the HTMH material system (without including the paired LTMH material) has been carried out comparing the techno-economic results with the targets. Only the HTMH materials that have the potential to meet or approach such targets have been selected to be paired with suitable LTMH materials. The materials (HTMH and LTMH) have been paired based on their properties (especially operating pressure) in order to avoid compression/expansion requirements to be included in the system. As a result, a large number of candidate materials were narrowed down to only a few HTMH-LTMH paired TES systems as possible final candidates. The selected TES systems have been examined and the techno-economic analysis has been carried out, with the data and degrees of freedoms values reported in Table 2.

The CSP plant characteristic values shown in Table 2 have been assumed based on the DOE targets for solar plants. Regarding the heat exchanger and pressure vessel assumptions, a typical (but conservative) value of MH materials improved thermal conductivity has been assumed [45,40]. The values of the diameter of the heat transfer fluid tube as well as the average temperature difference value between the fluid and the MH material have been assumed based on typical values for industrial applications. The value of the convective heat transfer coefficient (for both the HTMH and LTMH systems) has been assumed based on the typology of the solar plant, assuming the TES coupled to a high temperature solar receiver and a steam power plant. The U_{conv} for the HTMH system is on the same order of the values reported in the literature for high temperature heat transfer fluids, such as helium [37]. The U_{conv} for the LTMH system has been assumed equal to 2000 W/m^2K based on the fact the heat transfer fluid is condensing steam or water, which typically has heat transfer coefficients on the order of 1000–10000 W/m^2K or higher (for condensing fluid).

4. MH system screening

This section presents the results of the analyses carried out adopting the model described in Section 3.

4.1. The HTMH screening results

Results of the techno-economic analysis for the HTMH materials are reported in Figs. 4–7.

Fig. 4 shows the results obtained for the volumetric energy density of the selected HTMH materials. The results show that all of the materials can meet and exceed the target (25 $kWhth/m^3$), with the lowest value (for $NaMgH_3$ material) still being about 20 times higher than the target.

Fig. 5 reports the economic analysis results, showing the specific installed cost of the HTMH system, with the contribution of the material specific installed cost (C_{MS}) and the heat transfer system and pressure vessel specific installed cost (C_{HEPVS}). Four HTMH materials can meet the target of 15 $/kWhth. The results show that the heat transfer system and pressure vessel cost significantly influences the

Table 2
Baseline screening analysis data and assumptions.

CSP plant	*Heat exchanger and pressure vessel*
Wel = 100 MW	$D_1 = 0.015$ m
PCF = 63%	$k = 7$ W/mK
$\eta_{PP} = 45\%$	$U_{conv} = 2000$ W/m^2K
$\Delta t_s = 13$ h	$\Delta T = 25\,^{\circ}C$

Table 1
Properties of preliminary HTMH and LTMH selected materials for CSP applications.

	Working T/P (°C/bar)	**ΔH** (kJ/molH_2)	**ΔS** (kJ/molH_2 K)	**Theoretical wf** (wt% H_2)	**Bulk density** (kg/m^3)	**Raw material cost** ($/kg)	**References**
HTMH							
MgH_2	300–500/10–200	75	0.136	7.6	870	2.9	[41,42]
Mg_2FeH_6	350–550/10–200	77	0.137	5.5	1300	1.9	[21,42]
$NaMgH_3$	400–600/10–80	88	0.132	4.0	1000	4.2	[22,42,43]
LiH	950–1150/0.1–1.5	190	0.135	12.6	500	70.0	[44,42]
$TiH_{1.72}$	650–950/0.5–10	142	0.130	3.5	1600	12.0	[44,42]
CaH_2	900–1100/0.1–1.5	171	0.126	5.0	890	6.0	[44,42]
NaH	400–600/0.5–70	130	0.165	4.2	750	4.0	[44,43]
LTMH							
$TiFeH_2$	0–120/2–70	28	0.106	1.9	2500	7.0	[8,38]
$TiCr_{1.8}H_{3.5}$	0–70/85–600	20	0.110	2.4	2300	7.0	[8,38]
$TiMn_{1.5}H_{2.5}$	0–120/3–140	28	0.111	1.9	2200	6.0	[8,38]
$NaAlH_4$ (SAH)	80–120/10–60	40	0.132	5.6	750	3.2	[8,38,45,46]

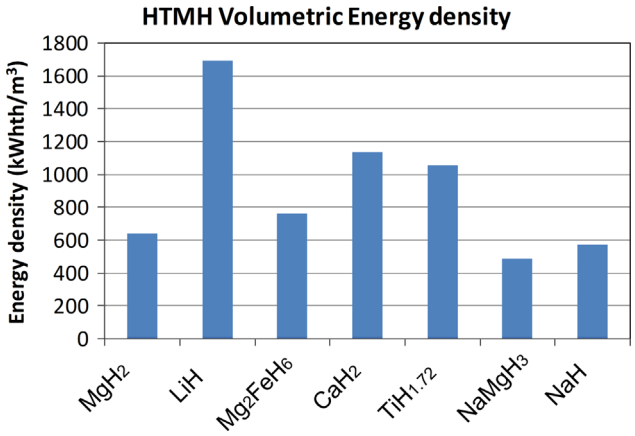

Fig. 4. HTMH system Volumetric Energy density (the energy density DOE target is 25 kWhth/m^3).

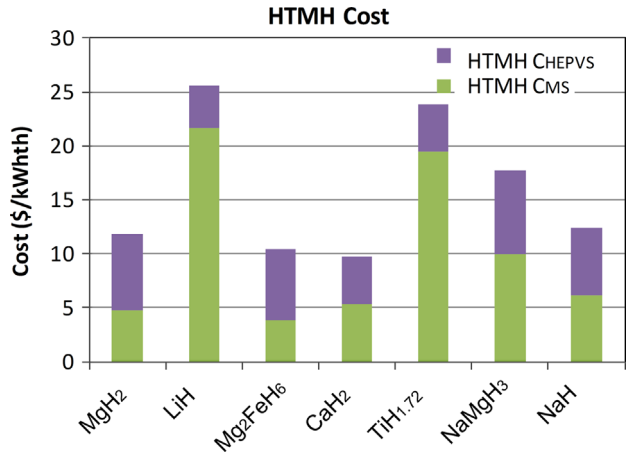

Fig. 5. HTMH system specific installed cost, comprising the material specific installed cost (C_{MS}) and the heat transfer system and pressure vessel specific installed cost (C_{HEPVS}).

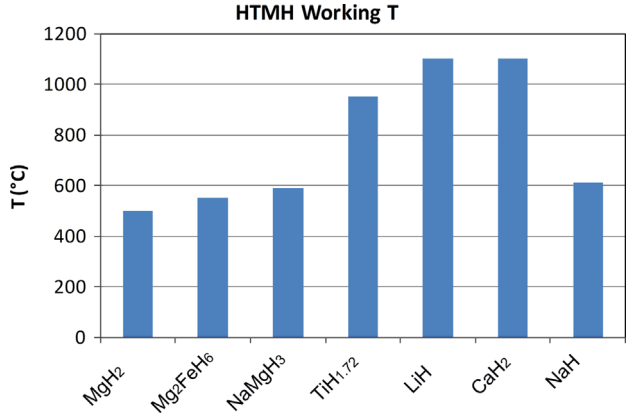

Fig. 6. HTMH materials typical operating temperatures.

overall cost of the low price and high pressure materials (Mg and Na family of materials). More than 60% of the HTMH cost is due to the heat transfer system and pressure vessel cost for MgH_2 and Mg_2FeH_6 materials. For the Na-based materials the overall cost is affected by the cost of heat exchanger and pressure vessel on the order of 45–50%. For low pressure materials, like the less expensive Ca-based system, the results show that the heat exchanger and pressure vessel affecting the overall cost by approximately 45–50%. Conversely, for the more

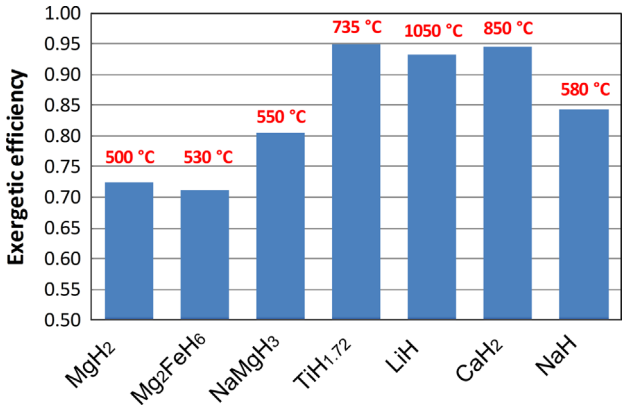

Fig. 7. HTMH system exergetic efficiency.

expensive low pressure materials (Li and Ti based MH's), the HTMH system cost is mainly affected by the material cost, with percentages on the order of 80–85%.

Figs. 6 and 7 show the typical operating temperatures and the corresponding exergetic efficiencies for the selected HTMH materials. Three material classes were identified. The first material class is comprised of Mg and Mg-Fe based materials. This class of materials is characterized by the lowest operating temperatures and highest pressure operating conditions. Their exergetic efficiency (for temperatures on the order of 500 °C) is on the order of 70–75%. These values can be higher at lower operating temperatures but at the expense of decreased power plant efficiency. The second material class is comprised of Na-based materials and it is characterized by higher operating temperatures, on the order of 550–600 °C, and pressures on the order of 50 bar. Typical exergetic efficiencies of these systems are around 85%. The last class of materials includes the very high temperature materials, with operating temperatures higher than 700 °C (reaching possible values greater than 1000 °C) and low operating pressures on the order of only a few bar. This class includes Ti, Li and Ca materials and has exergetic efficiencies on the order of 95%, allowing these materials to reach the exergetic efficiency targets at very high operating temperatures.

Based on the results obtained and with the goal of reaching a reasonable number of promising candidates, three HTMH systems were selected: (1) $NaMgH_3$ (or NaH or Mg_2FeH_6); (2) $TiH_{1.72}$; (3) CaH_2. The lowest temperature system is based on $NaMgH_3$ (or NaH or Mg_2FeH_6) material and operates at temperatures on the order of 500–550 °C. The MgH_2 material has been excluded due to its operating temperatures being too low to meet the targets, even at very high pressure. The second and the third systems operate at very high temperatures on the order of 700–900 °C, and are comprised of Ti-based material and Ca-based HTMH materials respectively. Li-based materials were excluded from further consideration based on their high cost.

4.2. *The selected TES systems results*

The three selected HTMH materials need to be paired with suitable LTMH materials in order to set up the complete TES system. While it has been found that the HTMH properties drive the overall operation of the MH TES system, it has also been found that often the LTMH material properties can strongly affect the overall MH TES system cost. Using the LTMH requirements discussed in Section 4.1 and the information on the LTMH materials in Table 1 a preliminary cost analysis, similar to the HTMH cost analysis was performed to narrow down the most promising LTMH candidates. In addition the correspondent LTMH, which exchanges hydrogen with the HTMH, needs to be adequately chosen based on the thermodynamic and kinetics

properties so as to avoid the addition of a hydrogen compression system. In particular, the SAH material can be paired only at a pressure on the order of 30–50 bar due to its kinetics properties [46]. Consequently the most promising HTMH being capable of being paired with SAH is the $NaMgH_3/Mg_2FeH_6$ system, while the low pressure HTMH materials (Ti and Ca based materials) can be paired best with a Ti-based LTMH material. Thus the final three coupled material candidate systems are

- $NaMgH_3$ (or NaH or Mg_2FeH_6)–SAH
- $TiH_{1.72}$–TiFe
- CaH_2–TiFe

The TES system volumetric energy density for the paired systems is shown in Fig. 8. Results show that all the selected systems can meet and exceed the target (25 kWhth/m^3). The lowest volumetric energy density system shows a value about 8 times higher than that of the target.

Preliminary economic analysis results reported in Fig. 9, show the specific installed cost of the three selected systems. The contribution of material cost (C_{MS}) and the heat exchanger and pressure vessel cost (C_{HEPVS}) for the HTMH and LTMH systems are shown.

The pairs with the lowest costs are those with SAH as the LTMH material or those with CaH_2 as the HTMH material. This is due to the low material specific cost and the advantageous thermochemical properties of these materials. For the $NaMgH_3$-SAH pair, the overall HTMH cost represents approximately 47% of the system cost, which includes the material cost, the heat transfer system and the pressure vessel. The comparable LTMH cost is approximately 53% of the overall cost with 43% of this LTMH cost due to the heat transfer and pressure vessel system and the remainder due to the material cost. According with the results reported in Fig. 5, the influence of the heat exchanger and pressure vessel cost is mainly due to the high operating pressure and to the intrinsic characteristics of the two MH's.

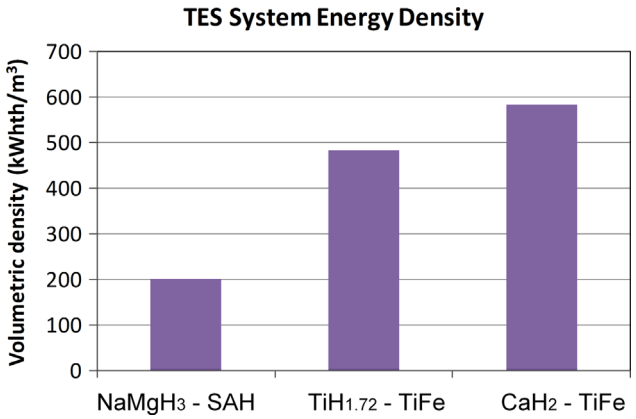

Fig. 8. TES systems volumetric energy density.

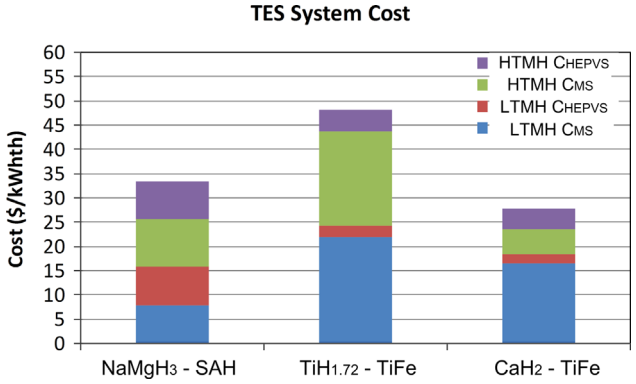

Fig. 9. TES system specific installed cost. The material due specific installed cost (C_{MS}) and the heat transfer system and pressure vessel specific installed cost (C_{HEPVS}) are shown for both HTMH and LTMH system.

The low pressure material pairs, which use Ti-based LTMH materials, show a significant influence of the LTMH material cost on the overall system cost. Regarding the $TiH_{1.72}$-TiFe couple, the influence of the HTMH and LTMH system costs on the overall system cost is approximately the same (50%), because of the comparable weight capacity of the two materials and of the similar specific material costs. The largest cost fractions for this system are due to the materials (both HT and LT) which represent almost 86% of the total cost. The CaH_2-TiFe pair is the lowest cost couple. Most of the cost is due to LTMH system (66% of the overall cost), since TiFe based material is more expensive than Calcium

4.3. Sensitivity analysis results

Based on the results obtained, several sensitivity analyses were performed for the selected MH couples. The influence of several factors affecting the system cost is depicted in Figs. 10–12 for the three selected TES systems. These factors are the concentrated solar power (CSP) plant performance parameters (PCF and storage time, as well as η_{PP}) and TES system techno-economic parameters (material price, material heat of reaction, thermal conductivity and heat exchanger and pressure vessel cost). The sensitivity analysis has been conducted by varying each parameter between the minimum and maximum values, indicated in the cost range included in the figures. The maximum and minimum values of the parameters have been assumed considering reasonable possible range variations. The material cost variation has been assumed based on possible price oscillations, different material purity levels, and on the properties of the material itself. Likewise, depending on the specific material, the variation of reaction enthalpy and weight capacity values has been assumed considering possible future material modifications. The thermal conductivity of the material has been varied within a suitable range, accounting for possible inclusion of different heat transfer enhancing systems as well as accounting for possible variation due to the contact resistance between metal hydride and tubes. The PP efficiency has been varied based on the operating temperatures of the TES system, as well as the PCF. PCF has also been varied within reasonable ranges, corresponding to variation of the storage time.

Fig. 10 shows the results obtained for the NaMgH3-SAH pair. The baseline case parameters for the pair are: HTMH material price=4.15 $/kg, LTMH material price=3 $/kg, HTMH ΔH=88 kJ/mol, LTMH ΔH=40 kJ/mol, HTMH wf=4.0%, LTMH wf=3.7%, k=7 W/mK, PP efficiency=45%, PCF=63%.

The material cost and the HTMH material heat of reactions have the most influence on the overall system cost. A variation of HTMH and LTMH material cost of 50% results in a TES system cost variation of 15% (HTMH) and 12% (LTMH), respectively. The heat of reaction variation has an influence on the specific cost of the HTMH and LTMH materials, as well as on the heat transfer systems. The influence of the HTMH heat of reaction is higher than that of the LTMH, since it determines the amount of hydrogen to be stored. In addition, results show that the heat transfer and pressure vessel system cost variation has a strong impact on the overall specific cost. A variation of 40% of the cost of the pressure vessel (either HTMH or LTMH) results in a variation of approximately 10% of the system cost.

Fig. 11 shows the results obtained the TiH1.72-TiFe pair. The baseline case parameters for the pair are: HTMH material price=11.5 $/kg, LTMH material price=7 $/kg, HTMH ΔH=142 kJ/mol,

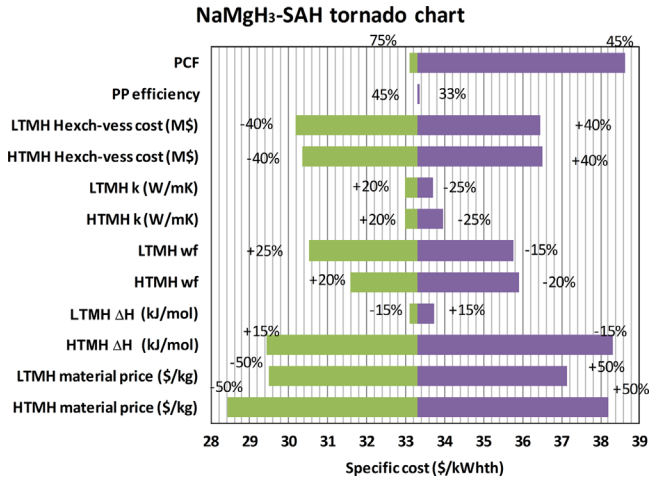

Fig. 10. $NaMgH_3$–SAH pair tornado sensitivity chart with variation of the CSP and material characteristic parameters (the minimum and maximum values of the parameters are indicated). The baseline case parameters are: HTMH material price=4.15 $/kg, LTMH material price=3 $/kg, HTMH ΔH=88 kJ/mol, LTMH ΔH=40 kJ/mol, HTMH *wf*=4.0%, LTMH wf=3.7%, *k*=7 W/mK, PP efficiency=45%, PCF=63%.

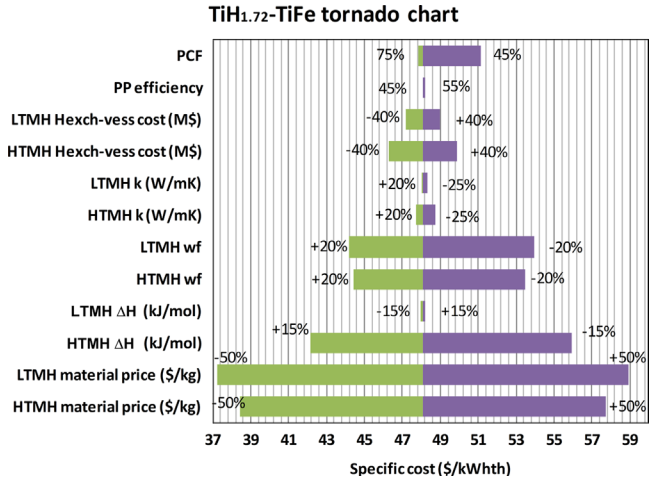

Fig. 11. $TiH_{1.72}$–$TiFeH_2$ pair tornado sensitivity chart with variation of the CSP and material characteristic parameters (the minimum and maximum values of the parameters are indicated). The baseline case parameters are: HTMH material price=11.5 $/kg, LTMH material price=7 $/kg, HTMH ΔH=142 kJ/mol, LTMH ΔH=28 kJ/mol, HTMH *wf*=3.5%, LTMH wf=1.9%, *k*=7W/mK, η_{PP}=45%, PCF=63%.

LTMH ΔH=28 kJ/mol, HTMH *wf*=3.5%, LTMH *wf*=1.9%, *k*=7W/mK, η_{PP}=45%, PCF=63%. The HTMH material cost and the HTMH material heat of reaction have the highest impact on the overall system cost. An increase of HTMH and LTMH material price of 50% results in a TES system cost variation of 20% (HTMH) and 22.5% (LTMH), respectively. The heat of reaction variation has an influence on the material cost (both HTMH and LTMH systems), as well as on the heat transfer system cost. The influence of the HTMH heat of reaction is again predominant compared to that of the LTMH, since it determines the amount of hydrogen to be stored. A decrease of the HTMH heat of reaction of 15% results in an increase in the overall cost of more than 16%. A variation of the weight capacity of the HTMH material also influences the overall cost. A decrease of 20% of the HTMH weight capacity value results in an increase of about 11% of the cost. On the other hand, the influence of the heat transfer system cost on the overall cost is less important than the $NaMgH_3$-based system. A variation of the pressure vessel cost determines a lower variation of the system cost.

Fig. 12 shows the results obtained for the CaH_2-TiFe pair. The baseline case parameters for the pair are: HTMH material price=6

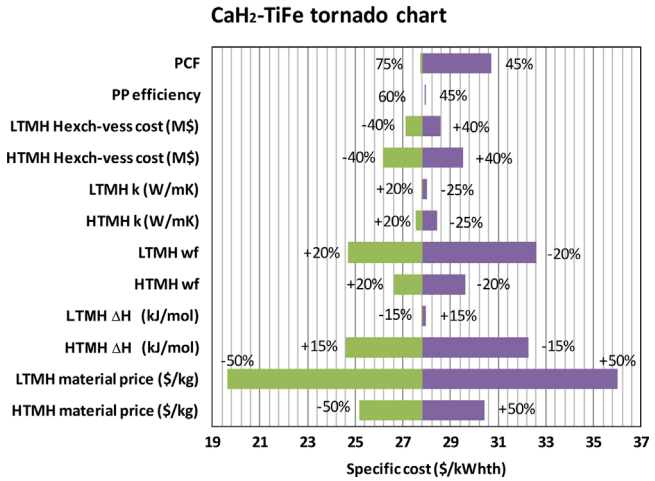

Fig. 12. CaH_2–$TiFeH_2$ pair tornado sensitivity chart with variation of the CSP and material characteristic parameters (the minimum and maximum values of the parameters are indicated). The baseline case parameeers are: HTMH material price=6 $/kg, LTMH material price=7 $/kg, HTMH ΔH=188 kJ/mol, LTMH ΔH=28 kJ/mol, HTMH *wf*=5.0%, LTMH *wf*=1.9%, *k*=7 W/mK, η_{PP} =45%, PCF=63%.

$/kg, LTMH material price=7 $/kg, HTMH ΔH=188 kJ/mol, LTMH ΔH=28 kJ/mol, HTMH *wf*=5.0%, LTMH wf=1.9%, *k*=7 W/mK, η_{PP} =45%, PCF=63%. Similar to the results shown in Fig. 9 the main influence on the overall system cost is due to the LTMH material cost. This cost is determined by the LTMH price, the HTMH heat of reaction and the LTMH hydrogen capacity, which represent the main properties affecting the overall system cost. For this material pair, a variation of the LTMH material price of 50% results in a system cost variation of about 30%. This price variation is realistic, noting that the price of iron-titanium has continuously been decreasing for 2–3 years [42] reaching (end of 2013) a price about 13% lower than the baseline price adopted in the current work. A decrease of the HTMH heat of reaction of 15% results in an increase of the overall cost of approximately 11.5%. A variation of the weight capacity of the LTMH material also influences the overall cost with a cost decrease of more than 11% correspondent to an increase of the weight capacity of 20%. On the other hand, the HTMH material properties have less effect on the overall system cost, due to the lower cost of the HTMH material.

5. Metal hydride TES status and future outlook

Based on information from the review of previous work and the results obtained from the screening analysis, some of today's MH-based TES systems show the potential to meet many of the DOE targets, even exceeding some of them. The MH TES system shows specific installed costs on the same order of those for molten salt, which represents the baseline TES system technology, in the range of 25–40 $/kWhth [47]. MH technology can also achieve high operating temperatures, high exergetic efficiency and high volumetric capacity, meeting and often exceeding the correspondent DOE targets, as demonstrated by the current analysis. However the ultimate TES system needs to meet all the DOE targets in order to be part of a CSP plant system which can achieve the ultimate economic target represented by the electricity production cost equal to 0.06 $/kWh[5]. Presently some of the systems

[5] One of the other aspects is related to the cycling capacity of the materials. This aspect will be analyzed part of another publication with data for the different selected materials included and discussed. An additional cost related to hydride substitution and refurbishment should be included in the overall CSP plant economic and financial analysis to evaluate the final electricity cost.

included in the current screening analysis show a cost on the order of the target of 15 $/kWhth. However, the present analysis was carried out considering: (1) a shell and tube non-optimized heat exchanger approach and (2) only currently available non-modified MH materials. Detailed properties of many of the HTMH materials available today, especially those operating at very high temperatures, are not often available in the literature. This is due to the fact that the majority of the MH material studies carried out previously were aimed at automotive applications, which have completely different targets that are often the opposite to those needed for high temperature stationary thermal applications (e.g. low operating temperature, low reaction enthalpy). The presented review and the analysis herein are intended to be used as a guide for the needed additional research and development on high temperature materials for thermal driven stationary applications (CSP plants). The three selected MH based storage systems provide a starting point for future material and system development.

Results obtained for the low temperature and high pressure system show that the cost of the system is strongly influenced by both the material properties and the heat transfer system properties (both HTMH and LTMH systems). Future system development needs to be directed toward both material modification and heat transfer system improvement. For instance several material modifications to the Mg-based materials are being considered, adding additional elements that can result in higher reaction enthalpies, higher operating temperatures and lower raw material costs. Optimized finned tube heat transfer systems are also being considered for the current TES system, with the objective of reducing the heat transfer area and, ultimately, the component installed cost.

For the Ti/Ti–Fe system, the material cost (both HTMH and LTMH) represents the most influential factor on the system cost. This suggests that material modifications should be a high priority in the future development for this type of TES system. Several HTMH material modifications are being evaluated such as altering the hydride composition to increase the operating pressure as well as lowering the material cost. In particular an increase of the operating pressure is extremely beneficial from an economic point of view because the hydride could also be coupled with a less expensive LTMH (e.g. SAH).

Results obtained for the Ca/Ti–Fe system show that this system has the potential to achieve the economic target considering possible Ti–Fe material modifications that can reduce the cost of the material and the amount of hydrogen to be stored. In addition, possible Ca material modifications are also being studied, with the aim of increasing the operating pressure, which could result in a lower installed cost.

6. Summary and conclusions

A review of previous investigations was made on the use of metal hydrides for CSP TES applications. While some of the earlier investigators focused on very high temperature metal hydrides like Li- and Ca-based systems for space and other specialty applications, many of the more recent investigators looked at lower temperature and lower cost systems involving Mg-based materials for uses with commercial power systems. Later investigators also realized that the cost of the system would often depend on the cost and selection of the right LTMH material pair. This led to the search for various methods to lower the cost of rare-earth-type AB_5 and other high performing but high cost materials. Despite all of the previous studies no “ideal” MH TES system has been identified. Previous to the presented analysis no systematic study has been carried out that examines the latest metal hydride materials and evaluates their potential performance against today's performance and cost targets. Therefore, a screening analysis of potential candidate MH-based TES systems for large scale CSP plants was carried out to select the most promising (existing) metal hydrides. To do that a simplified techno-economic system model was developed to evaluate the performance of the system in terms of specific cost and the exergetic efficiency. The techno-economic modeling framework can be applied to different metal hydride-based systems, under different operating conditions, accounting for different heat transfer solutions. Three preliminary systems have been selected for future consideration based on their potential of achieving the DOE targets and their actual material pairing compatibility. The first system, based on an Mg-family material (e.g. Mg–Fe or Na–Mg based materials) or NaH material coupled with SAH material, works well for high pressures and low temperatures (approximately 500–550 °C) applications. The second system couples Ti-based HTMH material with Ti-Fe based LTMH material. It works well at low pressures and high temperatures on the order of 700 °C. The third system couples Ca-based HTMH material and Ti-Fe LTMH material. The system works well at low pressure and very high temperatures (on the order of 800–1000 °C) for high efficiency power plants, resulting in potentially very low CSP system costs. Currently some of the selected systems are capable of approaching the DOE economic target for TES systems of 15 $/kWhth. Based on the results obtained from the screening analysis, several economic sensitivity analyses for the three selected systems were carried out. The screening analysis was mainly aimed at highlighting the influence of CSP plant operating conditions and MH system properties (e.g. material price, reaction enthalpy, and hydrogen capacity) on the TES specific installed cost. The most influential parameters have been highlighted for the three selected systems and the direction for future material and system improvements have been identified and discussed.

Acknowledgments

This work was performed as part of the DOE EERE SunShot Initiative. Dr L. Irwin, Sunshot Project Manager in appreciation for his help and direction. The authors also wish to thank Dr. S. Greenway (Greenway Energy LLC), Prof. C. Buckley and Dr. D. Sheppard (both Curtin University, Australia) for their useful suggestions and interactions.

Annex

The overall thermal energy stored in the TES system (E_{th}) is:

$$E_{th} = (W_{el}\Delta t_s)/(\eta_{PP}PCF) \quad (a1)$$

W_{el} is the average electric power produced by the plant during the year. Δt_s is the storage time, η_{PP} is the power plant efficiency and the PCF is the plant capacity factor

The cost of the MH material (C_M) has been evaluated based on the MH material weight. The hydrogen mass to be stored (M_{H2}) (i.e. moved from the HTMH to the LTMH and vice versa) can be evaluated as follows:

$$M_{H2} = (W_{el}\Delta t_s)/(\eta_{PP}PCF\Delta H_{HTMH}) \quad (a2)$$

ΔH_{HTMH} is the HTMH reaction enthalpy.

Consequently the mass of the HTMH (M_{HTMH}) and LTMH (M_{LTMH}) material can be assessed, once the weight capacity of the MH material (wf_{HTMH}) is known. The HTMH mass and volume (V_{HTMH}) are:

$$M_{HTMH} = M_{H2}/wf_{HTMH} \quad (a3)$$

$$V_{HTMH} = M_{HTMH}/\rho_{HTMH} \quad (a4)$$

ρ_{HTMH} is the HTMH material bulk density

The LTMH material mass (M_{LTMH}) and volume (V_{LTMH}) are evaluated once the material capacity (wf_{LTMH}) and bulk density

are known (ρ_{LTMH}):

$$M_{LTMH} = M_{H2}/wf_{LTMH} \quad (a5)$$

$$V_{LTMH} = M_{LTMH}/\rho_{LTMH} \quad (a6)$$

References

[1] Website: ⟨http://www.nrel.gov/csp/pdfs/48658.pdf⟩ [accessed April 2014].
[2] Gil A, Medrano M, Martorell I, Lazaro A, Dolado P, Zalba B, et al. State of the art on high temperature thermal energy storage for power generation part 1 – concepts, materials and modellization. Renew Sustain Energy Rev 2010;14:31–55.
[3] Stekli J, Irwin L, Pitchumani R. Technical challenges and opportunities for concentrating solar power with thermal energy storage. J Therm Sci Eng Appl 2013;5 (021011-021).
[4] Izquierdo S, Montanes C, Dopazo C, Fueyo N. Analysis of CSP plants for the definition of energy policies: the influence on electricity cost of solar multiples, capacity factors and energy storage. Energy Policy 2010;38(10):6215–21.
[5] Denholm P, Hand M. Grid flexibility and storage required to achieve very high penetration of variable renewable electricity. Energy Policy 2011;39(3):1817–30.
[6] D.O.E. ARPA-E High Energy Advanced Thermal Storage. DOE-FOA-0000471, 2011, available at ⟨https://arpa-e-foa.energy.gov/FileContent.aspx?FileID=79a5de09-8bfd-4590-9cb4-e42578248d90⟩ [accessed April 2014].
[7] Dominguez R, Baringo L, Conejo A. Optimal strategy for a concentrating solar power plant. Appl Energy 2012;98:316–25.
[8] Harries D, Paskevicius M, Sheppard D, Price T, Buckley C. Concentrating solar thermal heat storage using metal hydrides. In:Proceedings of the IEEE; 2012;100:pp.539–49.
[9] DOE SunShot. SunShot Vision Study – Chapter 5. February 2012.
[10] Bernauer O, Halene C. Properties of metal hydrides for use in industrial applications. J Less Common Met 1987;131(1–2):213–24.
[11] Bowman R, Fultz B. Metallic hydrides I: hydrogen storage and other gas-phase applications. MRS Bull 2002;27:688–93.
[12] Ronnebro E, Majzoub E. Recent advances in metal hydrides for clean energy applications. MRS Bull 2013;38:452–8.
[13] Caldwell RT, McDonald JW, Pietsch A. Solar-energy receiver with lithium-hydride heat storage. Solar Energy 1965;9:48–60.
[14] Hanold RJ, Johnston RD. Power plant heat storage arrangement. US Patent US3029596; 1962.
[15] Bogdanovic B, Ritter A, Spliethoff B. Active MgH_2–Mg systems for reversible chemical energy-storage. Angew Chem-Int Ed Engl 1990;29(3):223–34.
[16] Bogdanovic B, Hartwig TH, Spliethoff B. The devlopment, testing and optimization of energy-storage materials based on the MgH_2–Mg system. Int J Hydrog Energy 1993;18(7):575–89.
[17] Bogdanovic B, Hofmann H, Neuy A, Reiser A, Schlichte K. Ni-doped versus undoped Mg–MgH_2 materials for high temperature heat or hydrogen storage. J Alloys Compd 1999;292:57–71.
[18] Felderhoff M, Bogdanović B. High temperature metal hydrides as heat storage materials for solar and related applications. Int J Mol Sci 2009;10:325–44.
[19] Bogdanović B, Ritter A, Spliethoff B, Straßburger K. A process steam generator based on the high temperature magnesium hydride/magnesium heat storage system. Int J Hydrog Energy 1995;20:811–22.
[20] Wierse M, Werner R. Magnesium hydride for thermal energy storage in a small-scale solar-thermal power station. J Less Common Met 1991;172–174 (3):1111–21.
[21] Reiser A, Bogdanovic B, Schlichte K. The application of Mg-based metal-hydrides as heat energy storage systems. Int J Hydrog Energy 2000;25:425–30.
[22] Sheppard D, Paskevicius M, Buckley C. Thermodynamics of hydrogen desorption from $NaMgH_3$ and its application as a solar heat storage medium. Chem Mater 2011;23:4298–300.
[23] Bogdanović B, Reiser A, Schlichte K, Spliethoff B, Tesche B. Thermodynamics and dynamics of the Mg–Fe H system and its potential for thermochemical thermal energy storage. J Alloys Compd 2002;345:77–89.
[24] Harries D. A novel thermochemical energy storage technology. In: Proceedings of EcoGeneration Conference, Sydney, Australia; 2010.
[25] Yonezu I, Nasako K, Honda N, Sakai T. Development of thermal energy storage technology using metal hydrides. J Less Common Met 1983;89(2):351–8.
[26] Chumphongphan S, Paskevicius M, Sheppard D, Buckley C. Effect of Al and Mo substitution on the structural and hydrogen storage properties of $CaNi_5$. Int J Hydrog Energy 2013;38:2325–31.
[27] Libowitz, G.G. Thermal energy storage systems employing metal hydrides. US Patent: US4040410; 1977.
[28] Libowitz G, Blank Z. Solid metal hydrides: properties relating to their application in solar heating and cooling. In: Goodenough JB, Whittingham MS, editors. Solid State Chemistry of Energy Conversion and Storage. Washington, DC: ACS; 1976. p. 271–83.
[29] Bogdanovic B, Schwickardi M. Ti-doped alkali metal aluminum hydrides as potential novel reversible hydrogen storage materials. J Alloys Compd 1997;253–254:1–9.
[30] Motyka T. Savannah River National Laboratory Regenerative Fuel Cell Project. SRNL-STI-2008-00388; November 11, 2008.
[31] Guthrie KM. Data and techniques for preliminary capital cost estimating. Chem Eng Prog 1969:114–42.
[32] Douglas E. Industrial chemical process design. TX, USA: McGrw-Hill Professional Engineering; 2003.
[33] AspenTech. Aspen capital cost estimator, Version v8; December 2012.
[34] Szargut J. Exergy method technical and ecological applications. Southampton, UK: WIT Press; 2005.
[35] Szargut J. Egzergia Poradnik obliczania I stosowania. Gliwice: Widawnictwo Politechniki Shlaskej; 2007.
[36] Website: ⟨http://www.dlr.de/Portaldata/41/Resources/dokumente/institut/system/publications/Concentrating_Solar_Power_Part_1.pdf⟩ [accessed April 2014].
[37] Corgnale C, Summers W. Solar hydrogen production by the Hybrid Sulfur process. Int J Hydrog Energy 2011;36(18):11604–19.
[38] Buckley C. Personal communication. Australia: Curtin University; 2013.
[39] Buckley C, Sheppard D, Paskevicius M, Harries D. Metal hydrides for concentrated solar thermal (CST) applications. In: MCARE Conference 2012 Invited Talk.
[40] Pasini JM, Corgnale C, van Hassel B, Motyka T, Kumar S, Simmons K. Metal hydride material requirements for automotive hydrogen storage systems. Int J Hydrog Energy 2013;38(23):9755–65.
[41] Chaise A, De Rango P, Marty P, Fruchart D. Experimental and numerical study of a magnesium hydride tank. Int J Hydrog Energy 2010;35:6311–22.
[42] Website: ⟨http://www.metalprices.com/⟩ [accessed 2013].
[43] Di Pietro P, Skolnik E. Analysis of the Sodium Hydride-based hydrogen storage system. In: Proceedings of the 2000 Hydrogen Program NREL/CP-570-28890.
[44] Mueller W, Blackledge J, Libowitz G. Metal hydrides. New York and London: Academic Press; 1968.
[45] Corgnale C, Hardy BJ, Tamburello DA, Garrison SL, Anton DL. Acceptability envelope for metal hydride-based hydrogen storage systems. Int J Hydrog Energy 2012;37:2812–24.
[46] Hardy BJ, Anton DL. Hierarchical methodology for modeling hydrogen storage systems part II: detailed models. Int J Hydrog Energy 2009;34:2992–3004.
[47] Kolb G, Ho C, Mancini T, Gary J. Power tower technology roadmap and cost reduction plan. Sandia Report SAND2011-2419; April 2011.